4-3-2007

# Hybrid Automatic Repeat Requests for MB-OFDM Ultra-Wideband

Darryn Lowe
*University of Wollongong*, darrynl@uow.edu.au

Xiaojing Huang
*University of Wollongong*, huang@uow.edu.au

# Hybrid Automatic Repeat Requests for MB-OFDM Ultra-Wideband


## Abstract

This paper analyzes the design and performance of hybrid automatic repeat request (HARQ) extensions to the multi-band orthogonal frequency division multiplexing (MB-OFDM) ultra-wideband (UWB) standard. It is shown how both Type-I and Type-III HARQ can significantly reduce the packet error rate (PER) in realistic frequency-selective channels. An exhaustive search is used to find an optimal low-complexity Type-III HARQ scheme by deriving the distance spectra and bit error upperbound for all sets of complementary puncturing matrices. The consequences of selecting sub-optimal puncturing matrices are also quantified.



## Disciplines

Physical Sciences and Mathematics

## Publication Details

This paper was originally published as: Lowe, D & Huang, X, Hybrid Automatic Repeat Requests for MB-OFDM Ultra-Wideband, Third International Conference on Wireless and Mobile Communications 2007 (ICWMC '07), Guadeloupe, French Caribbean, 4-9 March 2007, 13-13.

# Hybrid Automatic Repeat Requests for MB-OFDM Ultra-wideband

Darryn Lowe and Xiaojing Huang
*Telecommunications Information Technology Research Institute*
*University of Wollongong*
*Northfields Avenue, Australia 2522*
{*darrynl, huang*}*@uow.edu.au*

***Abstract*— This paper analyzes the design and performance of hybrid automatic repeat request (HARQ) extensions to the multi-band orthogonal frequency division multiplexing (MB-OFDM) ultra-wideband (UWB) standard. It is shown how both Type-I and Type-III HARQ can significantly reduce the packet error rate (PER) in realistic frequency-selective channels. An exhaustive search is used to find an optimal low-complexity Type-III HARQ scheme by deriving the distance spectra and bit error upper-bound for all sets of complementary puncturing matrices. The consequences of selecting sub-optimal puncturing matrices are also quantified.**

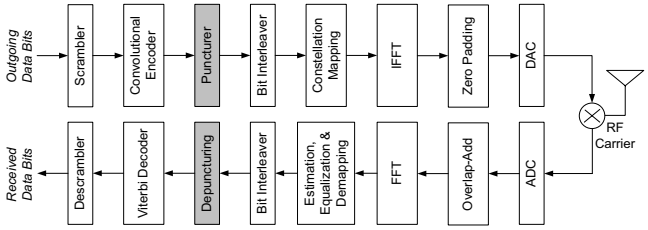


Fig. 1. OFDM transceiver block diagram.

## I. Introduction

Ultra-wideband (UWB) communication systems offer high-rate low-interference communication [1]. With UWB officially defined in 2002 by the United States Federal Communications Commission (FCC) as a signal with a 10 dB bandwidth of at least 500 MHz and a maximum equivalent isotropic radiated power spectral density (PSD) of no more than $-41.3$ dBm/MHz in the 3.1 – 10.6 GHz band [2], the race is on to exploit this untapped spectral resource.

The first UWB technology to be internationally standardized is multi-band orthogonal frequency division multiplexing (MB-OFDM) [3] developed by the WiMedia Alliance. The MB-OFDM standard defines both physical (PHY) and medium access control (MAC) layers and supports data rates from 53.3 Mbps to 480 Mbps. MB-OFDM divides the several gigahertz of spectrum allocated by the FCC into 14 bands, each with a 528 MHz bandwidth. These bands are then bundled into 5 band groups; only the first is mandatory.

MB-OFDM, which shares the generic OFDM block diagram of Fig. 1, has four distinguishing characteristics from previous OFDM wireless local area network (WLAN) standards such as IEEE 802.11a/g and HiperLAN/2. First, an MB-OFDM symbol is comprised of 128 samples rather than the 64 samples used in IEEE 802.11a. Second, a zero-pad (ZP) is used rather than a cyclic prefix (CP). Although a ZP leads to a higher peak-to-average power ratio, it is more efficient than a CP. Third, MB-OFDM supports a range of optional diversity improvements. This includes frequency domain spreading (FDS) and time domain spreading (TDS), both of which offer an extra 3 dB of process gain when activated, as well as dual carrier modulation (DCM) to combat frequency selective fading at high data rates. Fourth, time-frequency codes (TFCs) support optional time-frequency interleaving (TFI) to allow up to a 4.7 dB increase in peak transmit power. This is possible since if each 528 MHz band is active only for 1/3 of the time, the peak power radiated per-band can be up to 3 times higher without violating the $-41.3$ dBm/MHz FCC limit.

To reliably transfer information at a wide range of data rates, MB-OFDM combines a rate $\frac{1}{3}$ convolutional code with one of three optional puncturing matrices to yield net coding gains of $\frac{1}{3}$, $\frac{1}{2}$, $\frac{5}{8}$ and $\frac{3}{4}$. Since some packet errors are inevitable, the MB-OFDM standard also defines several automatic repeat request (ARQ) policies. In other words, a corrupted packet can be retransmitted by the MAC in order to protect sensitive higher-layer protocols such as TCP.

Since the puncturing pattern is constant for each data rate, we observe that a retransmitted MB-OFDM packet will be identical to the original. This means that a receiver can process a retransmitted packet in one of two ways. First, the receiver may ignore the original packet and consider the retransmission in isolation. Alternatively, the receiver may implement a hybrid ARQ (HARQ) scheme [4] wherein the information from both packets is combined in the hope of reducing the likelihood of a repeat error.

We begin this paper by reviewing HARQ techniques in Section II. Then, in Section III, we analyze the puncturing matrices used in the MB-OFDM standard and obtain optimal complementary matrices for a low-complexity Type-III HARQ scheme. Distance spectra and an upper-bound on theoretical performance are provided for each of the proposed puncturing matrices. Section IV then quantifies packet error rate (PER) via Monte-Carlo simulations. Our conclusions are presented in Section V.

Proceedings of the Third International
Conference on Wireless and Mobile Communications (ICWMC'07)
0-7695-2796-5/07 $20.00 © 2007 IEEE

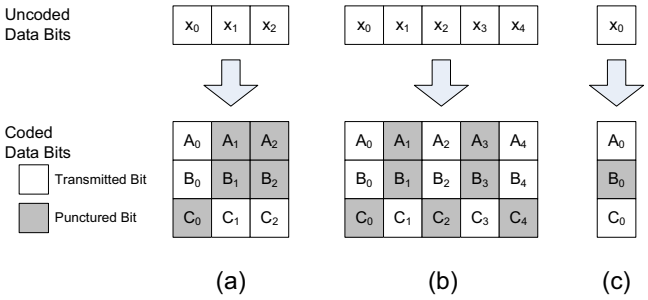


Fig. 2. Puncturing patterns (a) 480 Mbps, (b) 200 & 320 Mbps, (c) 80, 160 & 320 Mbps.

## II. HYBRID ARQ

There are three types of HARQ [4]. In Type-I HARQ, the retransmitted packet is identical to the original packet and the receiver combines both packets via maximal ratio combining (MRC). The advantage of Type-I HARQ is that both the original and retransmitted packets are self-decodable. This means that it is not necessary for the original packet to be available in order to correctly decode the retransmission. In Type-II HARQ, the retransmitted packet contains additional parity bits and is not self-decodable. Although Type-II HARQ can be more efficient, it requires a feedback channel via which the receiver can inform the sender of how many parity bits are needed. Type-III HARQ is a combination of Type-I and Type-II wherein the retransmitted packet remains self-decodable despite being coded differently from the original. In this paper, we do not consider Type-II HARQ since the extra communication adds complexity and latency that is unsuitable for high-rate multimedia-intensive UWB.

Implementing a Type-I HARQ scheme under the MB-OFDM standard is straight-forward. If a corrupted packet is received with its header intact, which is relatively likely given that the packet header is protected by Reed-Solomon forward error correction (FEC) in addition to the convolutional code used for the payload, then the soft-decision outputs from the demodulation process are retained. These are then combined the decision variables from the retransmitted packet when it arrives. If the decision variables are log-likelihood ratios (LLR), then we note that optimal MRC is purely additive and is therefore very low in computational complexity. Further, since the MB-OFDM MAC header includes both sequence numbers and an explicit retry bit, the current MB-OFDM standard implicitly supports Type-I HARQ.

To design an improved Type-III HARQ scheme, we begin by considering the punctured convolutional codes [5][6] that are used to select between the several data rates supported by the MB-OFDM standard. By using the data-rate specific puncturing matrices shown in Fig. 2, convolutional codes with gains of $\frac{3}{4}$, $\frac{5}{8}$ and $\frac{1}{2}$ are derived from a single rate $\frac{1}{3}$ mother code. By using a common mother code, the block diagram for which is shown in Fig. 3, the receiver needs only a single Viterbi decoder to support all data rates. This is done by having the receiver replace any punctured bits with soft-decision neutral 'zeros' prior to decoding.

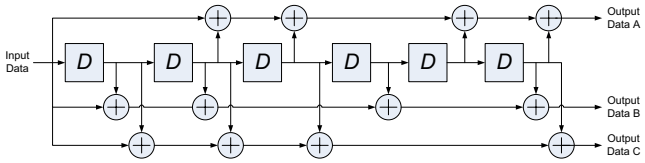


Fig. 3. Delay line for convolutional code.

A low-complexity Type-III HARQ scheme can therefore be obtained by modifying the puncturing matrix used for retransmitted packets. Note that although the existing PHY and MAC headers are sufficient if one ignores legacy support, full backwards compatibility with the current standard is easily maintained by using one the reserved bits in the PHY header. A '0' value for this bit would denote the use of the current puncturing matrices while a '1' would denote a modified puncturing matrix.

To find the optimal modified puncturing matrices for retransmitted packets at each data rate, we begin by denoting a general $R \times T$ puncturing matrix with $B$ transmitted bits as $\mathbf{P}^{(T,B)}$ where $R$ is the number of output bits per input bit of the mother convolutional code and $T$ is the puncturing period. For MB-OFDM, the rate $\frac{1}{3}$ mother code means that $R = 3$. Using this definition, the three puncturing patterns of Fig. 2 can be denoted as

$$\mathbf{P}_S^{(3,4)} = \begin{bmatrix} 1\,0\,0 \\ 1\,0\,0 \\ 0\,1\,1 \end{bmatrix} \quad \mathbf{P}_S^{(5,8)} = \begin{bmatrix} 1\,0\,1\,0\,1 \\ 1\,0\,1\,0\,1 \\ 0\,1\,0\,1\,0 \end{bmatrix} \quad \mathbf{P}_S^{(1,2)} = \begin{bmatrix} 1 \\ 0 \\ 1 \end{bmatrix} \qquad (1)$$

where the subscript $S$ denotes that the relevant puncturing matrix is specified in the MB-OFDM standard.

For an effective Type-III HARQ scheme, we need a complementary puncturing matrix that send some or all of the bits that were punctured by the original puncturing matrix. The advantage of this approach is that there is no increase in complexity since the modifications to the transmitter and receiver are localized to the puncturing stages highlighted in Fig. 1. Another advantageous feature is that it is guaranteed that the retransmitted packet will be the same size as the original. This avoids the need to reschedule channel access windows as could be the case for differently sized packets.

There are two criteria that define an optimal complementary puncturing matrix. First, the convolutional code that results from the MRC of the original and retransmitted packets must be optimal. This means that the number of punctured bits that are common to the original and complementary puncturing matrices must be minimized. Second, we must ensure that the convolutional code resultant from the modified puncturing matrix is not inferior to the original. This is critical to avoid sacrificing the self-decodability that defines Type-III HARQ. In the following section, we use an exhaustive search to identify the optimal complementary puncturing matrices that best meet these criteria.

## III. Optimal complementary Puncturing Matrices

In this section, we use an exhaustive search to find the optimal complementary puncturing matrices for all data rates in the MB-OFDM standard. This is done by deriving distance spectra and error rate upper-bounds. These complementary puncturing matrices are then used to implement an optimal Type-III HARQ scheme.

The rate $\frac{1}{3}$ mother code of Fig. 3 has a generator matrix

$$\begin{aligned}\mathbf{G}(D) &= \left[\begin{array}{ccc} A(D) & B(D) & C(D) \end{array}\right] \\ &= \left[\begin{array}{c} 1+D^2+D^3+D^5+D^6 \\ 1+D+D^2+D^4+D^6 \\ 1+D+D^2+D^3+D^6 \end{array}\right]^H \end{aligned} \quad (2)$$

where $[.]^H$ denotes the matrix transpose and $D$ denotes a delay of one sample period. To analyze the impact of various puncturing matrices, we first derive an expanded polyphase representation of the generator matrix. To that end, we start by considering each of the polynomials in the mother code's generator matrix individually.

Consider a single arbitrary polynomial $G(D)$ that can be decomposed into $T$ polyphase components $G_0^{(T)}(D)$ through $G_{T-1}^{(T)}(D)$. We can denote the relationship between the polyphase components and the original polynomial as

$$G(D) = \sum_{t=0}^{T-1} D^t G_t^{(T)}\left(D^T\right). \quad (3)$$

We can use these polyphase components to construct a *$T$-cyclic-phase elementary generator matrix*

$$\mathbf{\Gamma}_G^{(T)}(D) = \left[\begin{array}{ccccc} G_0(D) & G_1(D) & \ldots & G_{T-2}(D) & G_{T-1}(D) \\ DG_{T-1}(D) & G_0(D) & \ldots & G_{T-3}(D) & G_{T-2}(D) \\ \ldots & \ldots & \ldots & \ldots & \ldots \\ DG_1(D) & DG_2(D) & \ldots & DG_{T-1}(D) & G_0(D) \end{array}\right]. \quad (4)$$

We note that the generator matrix $\mathbf{\Gamma}_G^{(T)}(D)$ is functionality equivalent to the original polynomial $G(D)$, with the only difference being that it considers the input bits in blocks of $T$ rather than individually.

In the context of the MB-OFDM standard, where our original generator matrix is comprised of the three polynomials $A(D)$, $B(D)$ and $C(D)$, the equivalent *expanded generator matrix* of period $T$ can be denoted by concatenating the respective $T$-cyclic-phase elementary generator matrices $\mathbf{\Gamma}_A^{(T)}(D)$, $\mathbf{\Gamma}_B^{(T)}(D)$ and $\mathbf{\Gamma}_C^{(T)}(D)$. In other words,

$$\mathbf{G}^{(T)}(D) = \left[\begin{array}{ccc} \mathbf{\Gamma}_A^{(T)}(D) & \mathbf{\Gamma}_B^{(T)}(D) & \mathbf{\Gamma}_C^{(T)}(D) \end{array}\right]. \quad (5)$$

We reemphasize that the expanded generator matrix $\mathbf{G}^{(T)}(D)$ is functionally equivalent to the original generator matrix $G(D)$. For example, where the original generator matrix for the rate $\frac{1}{3}$ mother code in (2) defines a mapping of 1 input bit to 3 output bits, the expanded generator matrix $\mathbf{G}^{(T)}(D)$ defines a mapping of $T$ input bits to $3T$ output bits. The coding gain and distance spectra are unchanged.

The benefit of a $T \times RT$ expanded generator matrix is that it allow us to consider the effect of an $R \times T$ puncturing matrix $\mathbf{P}^{(T,B)}$. This is done by serializing $\mathbf{P}^{(T,B)}$ along each row, producing a $1 \times RT$ vector, and deleting the columns of the expanded generator matrix when the corresponding column in the serialized puncturing matrix is 0. For example, applying the $\mathbf{P}_S^{(3,5)}$ puncturing pattern from (1) to the expanded generator matrix of (9) would involve deleting the first, fourth, eighth and ninth columns.

The resultant *punctured expanded generator matrix* is then used to obtain the punctured convolutional code's free distance $d_f$ along with the distance spectra $a_n$ and $c_n$ [7]. This allows us to calculate an upper bound on the bit error probability [8] via

$$P_b \leq \sum_{d=d_f}^{\infty} c_d P_d \quad (6)$$

where $P_d$ is the probability that the wrong path at distance $d$ is selected. To simplify comparisons without loss of generality, we assume quadrature phase shift keying (QPSK) such that

$$P_d = \frac{1}{2}\mathrm{erfc}\left(\sqrt{d\frac{BE_B}{TN_0}}\right) \quad (7)$$

where $E_B$ is the energy per bit and $N_0$ is the noise power spectral density. We use this bound on probability of bit error rate as the principal criterion of goodness [9] when comparing candidate puncturing patterns.

### A. High-rate UWB

The 480 Mbps data rate in the MB-OFDM standard uses a $\frac{3}{4}$ rate convolutional code obtained via the puncturing pattern of Fig. 2a. By substituting $T = 3$ into (3), we can denote the polyphase components for the three polynomials in $G(D)$ as

$$\begin{array}{lll} A_0^{(3)}(D)=D^2+D+1 & B_0^{(3)}(D)=0 & C_0^{(3)}(D)=D+1 \\ A_1^{(3)}(D)=D^2+1 & B_1^{(3)}(D)=D+1 & C_1^{(3)}(D)=1 \\ A_2^{(3)}(D)=D^2+D+1 & B_2^{(3)}(D)=1 & C_2^{(3)}(D)=1 \end{array} \quad (8)$$

By using these polyphase components with (4), the $T = 3$ expanded generator matrix (9) can be obtained. This allows us to analyze any $3 \times 3$ puncturing matrix by removing the appropriate columns. For example, $P_S^{(3,4)}$ of Fig. the standard puncturing matrix of 2a would cause the removal of columns

$$\mathbf{G}^{(3)}(D) = \left[\begin{array}{ccccccccc} D^2+D+1 & 0 & D+1 & D^2+1 & D+1 & 1 & D^2+D+1 & 1 & 1 \\ D^2+D & D^2+D+1 & 0 & D & D^2+1 & D+1 & D & D^2+D+1 & 1 \\ 0 & D^2+D & D^2+D+1 & D^2+D & D & D^2+1 & D & D & D^2+D+1 \end{array}\right] \quad (9)$$

Proceedings of the Third International
Conference on Wireless and Mobile Communications (ICWMC'07)
0-7695-2796-5/07 $20.00 © 2007 IEEE

| Puncturing | [**P**] | $d_f$ | $(a_n \mid n = d_f, d_f+1, \ldots)$ $\{c_n \mid n = d_f, d_f+1, \ldots\}$ |
|---|---|---|---|
| Standard $\mathbf{P}_S^{(3,4)}$ | $\begin{matrix}1&0&0\\1&0&0\\0&1&1\end{matrix}$ | 5 | (28, 252, 1674, 11184, 65869, 393866) {4, 36, 175, 882, 4486, 23158} |
| Best $\mathbf{P}_B^{(3,4)}$ | $\begin{matrix}0&0&1\\0&1&1\\1&0&0\end{matrix}$ | 5 | (29, 238, 1410, 9045, 58299, 357938) {6, 33, 156, 781, 4134, 21658} |
| Worst $\mathbf{P}_W^{(3,4)}$ | $\begin{matrix}1&1&0\\0&0&1\\0&1&0\end{matrix}$ | 3 | (8, 31, 274, 1867, 10963, 64611) {1, 3, 26, 142, 689, 3537} |
| Best $\mathbf{P}_B^{(3,8)}$ | $\begin{matrix}1&1&1\\1&1&1\\0&1&1\end{matrix}$ | 12 | (7, 0, 78, 0, 314, 0, 1018, 0, 4266, 0, 16627, 0) {3, 0, 24, 0, 61, 0, 164, 0, 595, 0, 2036, 0} |
| Worst $\mathbf{P}_W^{(3,8)}$ | $\begin{matrix}1&1&0\\1&1&1\\1&1&1\end{matrix}$ | 12 | (4, 18, 37, 80, 169, 321, 383, 1207, 2418, 4177) {2, 7, 12, 18, 32, 53, 66, 181, 326, 562, 1087} |
| All $\mathbf{P}^{(3,9)}$ | $\begin{matrix}1&1&1\\1&1&1\\1&1&1\end{matrix}$ | 15 | (21, 24, 66, 132, 66, 282, 657, 846, 1593) {9, 9, 18, 27, 12, 54, 105, 135, 231, 459, 789} |

TABLE I

DISTANCE SPECTRA FOR SELECTED $T = 3$ PUNCTURING PATTERNS.

2, 3, 5, 6 and 7 (with the left-most column designated as column 1).

An exhaustive search of all puncturing matrices was conducted, with the distance spectra for several critical cases shown in Table I, with the subscript $S$ denoting a standard-specified puncturing matrix and subscripts $B$ and $W$ respectively denoting the best and worst puncturing matrices for the set defined by a given $T$ and $B$. For each puncturing matrix, the upper bound on bit error probability in an additive white Gaussian noise (AWGN) channel was calculated as per (7). The results are shown in Fig. 4.

We can make several observations from these results:

1) The standard puncturing matrix $\mathbf{P}_S^{(3,4)}$ is effectively optimal for the $\frac{3}{4}$ code rate since the exhaustive search revealed no superior matrices.
2) Since the best complementary puncturing matrix $\mathbf{P}_B^{(3,4)}$ yields a distance spectra that is almost equivalent to that of the original puncturing matrix, we meet the constraint that the retransmitted packet is self-decodable.
3) Poor selection of the puncturing pattern, such as the worst-case $\mathbf{P}_W^{(3,4)}$, can lead to extremely poor performance. This argues against the random bit selection proposed in [10].
4) A Type-III HARQ scheme can be over 1 dB better than a Type-I HARQ scheme, as shown by the difference between the best-case combined puncturing matrix $\mathbf{P}_B^{(3,8)}$ and the original matrix $\mathbf{P}_S^{(3,4)}$.
5) The difference between the best-case combined matrix $\mathbf{P}_B^{(3,8)}$ and the worst-case matrix $\mathbf{P}_W^{(3,8)}$ is trivial. This means that the location of the single punctured bit in the combined puncturing matrix is inconsequential and should not impact our selection of puncturing matrix for Type-III HARQ.

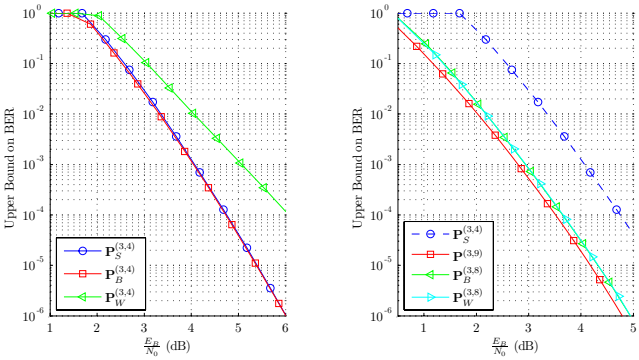


Fig. 4. BER for selected $T = 3$ puncturing patterns.

From these observations, our overall conclusion is that the optimal puncturing pattern for Type-III HARQ at 480 Mbps in MB-OFDM is $\mathbf{P}_B^{(3,4)}$.

### B. Mid-rate UWB

The 200 and 400 Mbps MB-OFDM data rates use a rate $\frac{5}{8}$ code obtained via the $T = 5$ puncturing pattern of Fig. 2b. By substituting $T = 5$ into (3), we can denote the polyphase components for the three polynomials in $G(D)$ as

$$\begin{array}{lll} A_0^{(5)}(D)=D+1 & B_0^{(5)}(D)=1 & C_0^{(5)}(D)=1 \\ A_1^{(5)}(D)=D & B_1^{(5)}(D)=D+1 & C_1^{(5)}(D)=D+1 \\ A_2^{(5)}(D)=1 & B_2^{(5)}(D)=1 & C_2^{(5)}(D)=1 \\ A_3^{(5)}(D)=1 & B_3^{(5)}(D)=0 & C_3^{(5)}(D)=1 \\ A_4^{(5)}(D)=0 & B_4^{(5)}(D)=1 & C_4^{(5)}(D)=0 \end{array} \quad (9)$$

Similar to the high-rate case, we can substitute these polyphase components into (4) to obtain the $T = 5$ expanded generator matrix (10). We then apply the puncturing matrix of $\mathbf{P}_S^{(5,8)}$,

$$\mathbf{G}^{(5)}(D) = \begin{bmatrix} D+1 & D & 1 & 1 & 0 & 1 & D+1 & 1 & 0 & 1 & 1 & D+1 & 1 & 1 & 0 \\ 0 & D+1 & D & 1 & 1 & D & 1 & D+1 & 1 & 0 & 0 & 1 & D+1 & 1 & 1 \\ D & 0 & D+1 & D & 1 & 0 & D & 1 & D+1 & 1 & D & 0 & 1 & D+1 & 1 \\ D & D & 0 & D+1 & D & D & 0 & D & 1 & D+1 & D & D & 0 & 1 & D+1 \\ D^2 & D & D & 0 & D+1 & D^2+D & D & 0 & D & 1 & D^2+D & D & D & 0 & 1 \end{bmatrix} \quad (10)$$

Proceedings of the Third International
Conference on Wireless and Mobile Communications (ICWMC'07)
0-7695-2796-5/07 $20.00 © 2007 IEEE

| Type | $[\mathbf{P}]$ | $d_f$ | $(a_n \vert n = d_f, d_f+1, \ldots)$ $\{c_n \vert n = d_f, d_f+1, \ldots\}$ |
|---|---|---|---|
| Standard $\mathbf{P}_S^{(5,8)}$ | 1 0 1 0 1<br>1 0 1 0 1<br>0 1 0 1 0 | 6 | (6, 81, 281, 1128, 4730, 17959, 66216, 246528, 911039)<br>{1, 19, 54, 153, 535, 1777, 5797, 19275, 64259} |
| Best $\mathbf{P}_{B_1}^{(5,8)}$ | 0 1 0 1 1<br>0 1 0 1 0<br>1 0 1 0 1 | 6 | (20, 67, 313, 1267, 4487, 18620, 75037, 269847, 969324)<br>{4, 16, 55, 171, 497, 1812, 6351, 20515, 66659} |
| Best $\mathbf{P}_{B_2}^{(5,8)}$ | 1 1 0 1 0<br>1 1 0 1 0<br>0 0 1 0 1 | 6 | (6, 81, 281, 1128, 4730, 17959, 66216, 246541, 911279)<br>{1, 19, 54, 153, 535, 1777, 5797 19276, 64280} |
| Best $\mathbf{P}_{B_1}^{(5,15)}$ | 1 1 1 1 1<br>1 1 1 1 1<br>1 1 1 1 1 | 15 | (35, 40, 110, 220, 110, 470, 1095, 1410, 2655, 5520)<br>{15, 15, 30, 45, 20, 90, 175, 225, 385, 765} |
| Best $\mathbf{P}_{B_2}^{(5,14)}$ | 1 1 1 1 1<br>1 1 1 1 1<br>0 1 1 1 1 | 12 | (3, 10, 10, 76, 150, 225, 338, 745, 1469, 2642)<br>{1, 4, 6, 24, 37, 45, 62, 124, 231, 387} |

TABLE II

DISTANCE SPECTRA FOR SELECTED $T = 5$ PUNCTURING PATTERNS.

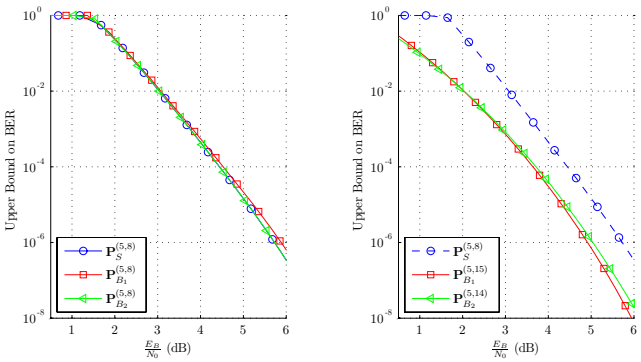


Fig. 5. BER for selected $T = 5$ puncturing patterns.

corresponding to Fig. 2b, by removing columns 2, 4, 7, 9, 11, 13 and 15.

After an exhaustive search over all puncturing patterns, the distance spectra and BER for the puncturing patterns of most interest are shown in Table II and Fig. 5 respectively. Unlike the high-rate case, where over half the bits were punctured, the mid-rate case is far less aggressive with 8 of each block of 15 bits being sent. This means that there will always be at least one bit common to any two $\mathbf{P}^{(5,8)}$ puncturing matrices. Since more than 2 bits of overlap will result in at least one bit being punctured from both matrices, we focus our search for the optimal complementary puncturing matrix to cases with overlaps of 1 and 2 bits, denoted as $\mathbf{P}_{B_1}^{(5,h_1)}$ and $\mathbf{P}_{B_2}^{(5,h_2)}$ respectively. This allows us to consider both self-decodability, where $h_1 = h_2 = 8$, as well as MRC scenarios, where $h_1 = 15$ and $h_2 = 14$.

We make several observations from these results:

1) If we restrict the overlap between the transmitted and retransmitted packets to only 1 bit, the optimal puncturing matrix $\mathbf{P}_{B_1}^{(5,8)}$ results in a degradation of 0.15 dB relative to the standard puncturing pattern $\mathbf{P}_S^{(5,8)}$.
2) If we restrict the overlap between the transmitted and retransmitted packets to 2 bits, the optimal puncturing pattern $\mathbf{P}_{B_2}^{(5,8)}$ incurs no loss.
3) After MRC, the case with a 2 bit overlap has a 0.14 dB advantage over the case with a 1 bit overlap.

| Puncturing | $[\mathbf{P}]$ | $d_f$ | $(a_n \vert n = d_f, d_f+1, \ldots)$ $\{c_n \vert n = d_f, d_f+1, \ldots\}$ |
|---|---|---|---|
| Standard $\mathbf{P}_S^{(1,2)}$ | 1<br>0<br>1 | 10 | (36, 0, 211, 0, 1404, 0, 11633, 0, 77433 0)<br>{11, 0, 38, 0, 193, 0, 1331 0, 7275, 0} |
| Best $\mathbf{P}_B^{(1,2)}$ | 1<br>1<br>0 | 8 | (3, 0, 25, 0, 268, 0, 1983, 0, 12516, 0)<br>{1, 0, 6, 0, 47, 0, 244, 0, 1308, 0} |

TABLE III

DISTANCE SPECTRA FOR SELECTED $T = 1$ PUNCTURING PATTERNS.

We conclude that the optimal puncturing matrix for retransmissions under Type-III HARQ at the 200 and 400 Mbps data rate is $\mathbf{P}_{B_2}^{(5,8)}$. Although the 1-bit overlap case gives marginally better performance after packet combining, its inferior performance when considered individually is an unacceptable tradeoff.

### C. Low-rate UWB

The 80, 160 and 320 Mbps MB-OFDM data rates use a rate $\frac{1}{2}$ code obtained via the $T = 1$ puncturing matrix of Fig. 2c. Since there is no need for a polyphase expansion, the expanded generator matrix is equivalent to the original generator matrix (2). Since there are only three possible realizations of $\mathbf{P}^{(1,2)}$, it is obvious that the MRC of any two different puncturing matrices will result in all bits being sent with at least one bit of overlap.

As shown in Table III, the optimal puncturing matrix is clearly that recommended by the standard.

Further, we observe that the free distance of the best complementary puncturing matrix is considerably less than that of the original puncturing matrix. This means there is no acceptable Type-III HARQ scheme since it is not possible to have a retransmitted packet that has a similar level of self-decodability.

## IV. RESULTS

Monte-Carlo simulations were used to quantify the end-to-end performance under the widely-accepted IEEE 802.15.3a UWB channel models [11]. Fig. 6 and Fig. 7 show the high-rate and mid-rate performance respectively, with the packet error rate (PER) based on packets of 1500 octets. We observe that while both Type-I and Type-III HARQ schemes offer improvements over the baseline case, the superiority of a Type-III HARQ scheme is particulary noticeable at low signal-to-noise ratios. Given that there is no appreciable increase in transceiver complexity from having a variable puncturing

Proceedings of the Third International
Conference on Wireless and Mobile Communications (ICWMC'07)
0-7695-2796-5/07 $20.00 © 2007 IEEE

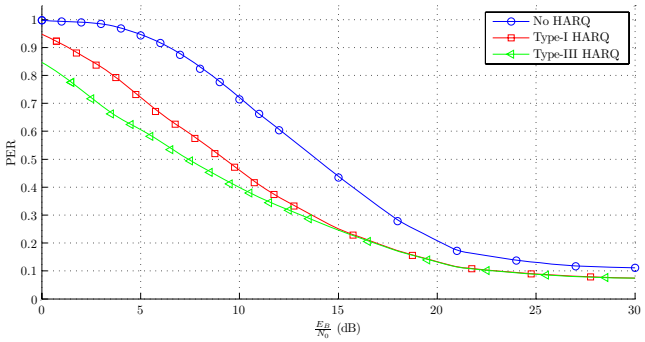


Fig. 6. 480 Mbps performance in channel model 1.

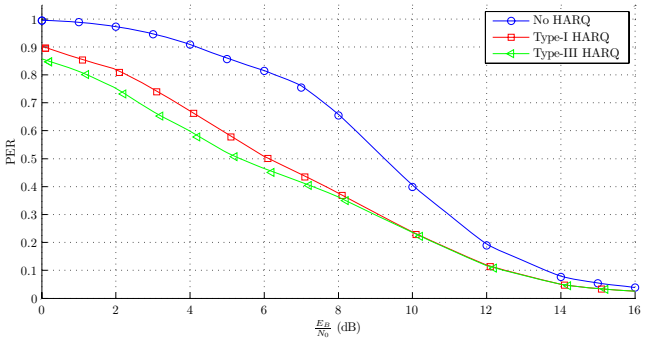


Fig. 7. 400 Mbps performance in channel model 3.

matrix, we conclude that Type-III HARQ is an easy means for improving real-world performance.

## V. Conclusions

In this paper, we investigated Type-I and Type-III HARQ techniques in the context of the MB-OFDM UWB standard. We identified optimal complementary puncturing matrices that allow a Type-III HARQ scheme to be implemented at no increase in transceiver complexity. Performance was analyzed both theoretically and through simulations, with the results showing significant improvements in real-world multipath channels.

## References

[1] K. Siwiak and D. McKeown, *Ultra-wideband Radio Technology*. Chichester, England: Wiley and Sons, 2004.

[2] *First Report and Order, Revision of Part 15 of the Commission's Rules Regarding Ultra-Wideband Transmission Systems*, Federal Communications Commission ET Docket 98-153, Feb. 2002.

[3] A. Batra, J. Balakrishnan, G. R. Aiello, J. R. Foerster, and A. Dabak, "Design of a multiband OFDM system for realistic UWB channel environments," in *IEEE Transactions on Microwave Theory and Techniques*, vol. 52, no. 9, Sept. 2004, pp. 2123–2138.

[4] Y. J. Guo, *Advances in Mobile Radio Access Networks*. Norwood, USA: Artech House Publishers, 2004.

[5] Y. Yasuda, K. Kashiki, and Y. Hirata, "High-rate punctured convolutional codes for soft decision Viterbi decoding," *IEEE Trans. Commun.*, vol. COM-32, pp. 315–319, Mar. 1984.

[6] D. Haccoun and G. Begin, "High-rate punctured convolutional codes for Viterbi and sequential decoding," *IEEE Trans. Commun.*, vol. 37, pp. 1113–1125, Nov. 1989.

[7] M. Cedervall and R. Johannesson, "A fast algorithm for computing distance spectrum of convolutional codes," *IEEE Trans. Info. Theory*, vol. 35, no. 6, pp. 1146–1159, Nov. 1989.

[8] A. J. Viterbi and J. K. Omura, *Principles of Digital Communication and Coding*. New York, USA: McGrow Hill, 1979.

[9] J. Hagenauer, "Rate-compatible punctured convolutional codes (RCPC codes) and their applications," *IEEE Trans. Commun.*, vol. 36, no. 4, pp. 389–400, Apr. 1988.

[10] E. Soljanin, R. Liu, and P. Spasojevic, "Hybrid ARQ with random transmission assignments," *Advances in Network Information Theory*, vol. 66, 2004.

[11] A. F. Molisch, J. R. Foerester, and M. Pendergrass, "Channel models for ultrawideband personal area networks," *IEEE Wireless Commun. Mag.*, pp. 14–21, Dec. 2003.

Proceedings of the Third International
Conference on Wireless and Mobile Communications (ICWMC'07)
0-7695-2796-5/07 $20.00 © 2007 IEEE